Comprehensive Cost Minimization for Charging Electric Bus Fleets

Daniel Mortensen, Jacob Gunther, Greg Droge, Justin Whitaker

***Abstract*—Recent attention to reducing carbon emissions have pushed transit authorities to adopt battery electric buses (BEBs). Two challenges associated BEB are extended charge times, which create logistical challenges and may force BEBs to charge when energy is more expensive. Furthermore, BEB charging leads to high power demands, which can significantly increase monthly power costs and may push electricity distribution circuits beyond their present capacity, revealing hidden costs of BEB adoption. This work presents a comprehensive method for minimizing the monthly cost incurred by charging BEBs while meeting bus route constraints, accounting for uncontrolled loads and both daytime and overnight charging, explores multiple charge rates, and minimizes a realistic cost model. A graph-based network-flow framework encodes the charging action space, physical constraints of buses, and represents the dynamics of bus battery state of charge. A mixed integer linear program is derived from the graph. Optimal charging schedules are explored in three scenarios: uncontested charging (equal numbers of buses and chargers), contested charging (more buses than chargers), and variable rate comparisons. Among other findings, we show that BEBs can be added to the fleet for only the cost of the energy to charge them but without raising the peak power demand, suggesting that conversion to electrified transit without expensive upgrades to the electrical infrastructure.**

***Index Terms*—Battery Electric Buses, Cost Minimization, Multi-Rate Charging, Mixed Integer Linear Program**

I. Introduction

Recent calls for a reduced carbon footprint have led transit authorities to adopt battery electric buses (BEBs). Replacing diesel and CNG buses with BEBs reduces environmental impact [21] as BEBs provide zero vehicle emissions and can access renewable energy sources[14].

Charging BEBs draws power from electrical infrastructure. The combined effect of BEB charging with other necessary loads can exceed the capacity of local distribution circuits [17][6][3], leading to the necessity of making expensive infrastructure upgrades. Power providers pass along to customers the cost of upgrades. Thus, the benefits of large-scale adoption of electrified bussing seem appealing at first, but public acceptance of electrified bussing is practical only if costly upgrades to the infrastructure can be deferred or avoided altogether.

One approach to deferring or avoiding upgrades is to intentionally managing the bus charging schedule including when and at what rates buses should charge. An optimal charge plan must account for a number of physical constraints and operational realities. For example, buses must exceed a minimum charge level while adhering to route schedules. When charging, batteries must be provided sufficient time to charge, and buses share a limited number of chargers. Moreover, charging takes place while other services draw power from the grid. Hereafter, these other loads are called "uncontrolled loads". The focus of this work is to find an optimal charge schedule which meets these requirements and minimizes the cost of electricity and grid impacts in the presence of uncontrolled loads. This problem is referred to hereafter as the "charge problem".

The remainder of this paper is organized as follows: Section II describes prior related work and Section III outlines a graph-based framework for modeling the environment including buses, routes, chargers, and uncontrolled loads. Section IV incorporates the problem constraints involving battery charge dynamics and Section V extends the the graph framework to account for differences between day and night operations. Sections VI translate the rate schedule used for billing into an objective function. Finally, Sections VII and VIII present results and describe future work, respectively.

II. Literature Review

This section summarizes prior work related to the charge problem and includes discussion on battery charging and managing runtime costs. The final subsection discusses the contributions of this paper, and how they relate to prior methods.

A. Battery Charging

Recharging BEBs is more time consuming than refueling diesel and CNG buses [18]. A diesel or CNG engine can refuel in several minutes but an electric bus may require several hours to charge, making the extended charge time a primary impediment in converting to BEBs.

To circumvent long refuel times, [20] and [11] propose an approach which replaces batteries when the state of charge is low. The exchange would replace the current battery with one that was fully charged and return spent batteries to recharge afterward. Exchanging batteries reduces down time, but is non-trivial because battery swapping requires specialized tools and/or automation.

Another alternative is to inductively charge buses while they are in motion. Dynamic charging simplifies logistics because it eliminates the time involved in stationary charging. Both [2] and [12] propose methods that inductively charge BEBs using specialized hardware in the road. A technique developed by [5] provides a planning framework for in-road charger placement that maximizes the benefits of dynamic charging. The method proposed in this paper can leverage in-road

dynamic charging where it exists. However, the framework is developed assuming stationary charging at a bus station.

Recharging BEBs at a station requires only the development of an intelligent charge schedule. Following a charge schedule requires minimal modifications to charging infrastructure and utilizes existing charging ports in the BEBs with no need for additional tools or automation. Algorithms for planning use foreknowledge of the runtime environment and battery dynamics to identify when and to which buses chargers should connect. Planning algorithms discussed in this review are considered on a scale from "reactive" to "global", where reactive methods respond to stimuli at the present, and global techniques use complete knowledge about the operating environment to form a plan.

Because reactive planning generally focuses on present circumstances, it requires minimal knowledge of the operational environment, making reactive planning extremely versatile. Methods of this type are both computationally efficient and adapt to many use cases. One such example is illustrated in [4], which splits the total power draw between the grid and an external battery to regulate the instantaneous load.

Reactive algorithms can be enhanced by encoding details for future events to improve decision making. If only event details within a finite horizon are used, the algorithm becomes a hybrid, containing features of both reactive and global techniques. For example, [1] describes a technique for optimizing a charging schedule out to a scheduling horizon. Changing the horizon adjusts both the scope and computational complexity of the solution. In stochastic environments, a smaller window is beneficial as charge schedules must be frequently recomputed, whereas in more stable circumstances, longer windows can yield improved performance.

Global algorithms include information from all time periods out to a predetermined end time. Because global algorithms assume complete foreknowledge of future events, they provide globally optimal plans and achieve the highest performance. The authors of [10] provide a technique which assumes foreknowledge of the current grid use. The grid schedule is encoded in the algorithm to inform optimal charging periods. Both [19] and [7] assume that bus schedules are known a priori and use this knowledge to stagger charge times to meet operational constraints.

B. Cost Optimization

In addition to physical constraints such as bus routes and charging dynamics, this paper focuses on minimizing the cost associated with charging and minimizes over fees assessed for on and off-peak energy use, on and off-peak power demand, and facilities power charges [16]. Prior work has dealt with charge costs in various ways. The authors in [8] propose a method to forecast power use. Work done by [15] propose a method which reduces the demand charge by using power forecasts to plan charge times[8]. When forecasting is not possible, both [13] and [4] propose methods that decreases power demand by observing the load and drawing additional power from on-site battery packs. Additionally, [7] minimized over on/off peak energy as part of their work.

C. Contributions

This paper develops a comprehensive charge schedule planning framework which extends the planner proposed by [19] to include multi-rate charging, uncontrolled loads, night/day charging, and a realistic rate schedule in [16]. Our method formulates the bus charge problem as a Mixed Integer Linear Program (MILP) and is unique because the objective function is the cost for the transit authority (bus fleet operator) and includes charges for on-peak and off-peak energy use, on-peak and off-peak power demand, and facilities demand. The proposed framework handles contention for charging resources in a globally optimal manner which guarantees charger availability even when chargers are scarce.

Prior work has also made assumptions for night time charge behavior. Our work eliminates the need for such by including both day and night charging in the charge schedule optimization. The modeling of night and day charging also includes their respective operational constraints such as charge rates, bus availability, and the number of available chargers.

Our work also seeks to understand how variable rate, as compared to single rate charging, affects the cost optimality and contributes a more accurate representation of battery charging dynamics.

The final contribution is recognizing that our framework provides a tool that enables prediction of monthly costs for transit authorities and infrastructure demand for power providers. Optimized charging schedules reduce power demand and extend use of current electrical infrastructure.

III. Graph Based Problem Formulation

This section formulates the charge problem as an optimization problem where the variables are defined in a graph. The first subsection describes the intuition behind this graph-based approach and the second develops a series of equality and inequality constraints resulting in a Mixed Integer Linear Program (MILP).

A. Graph Formulation

A solution to the bus charge problem is a schedule of actions for charging equipment. A schedule states both *when* and *which* bus a charger should connect, suggesting a model with two dimensions. The first dimension represents time and is given discretely in a left to right fashion. The second dimension encodes the charger state and extends vertically as shown in figure 1. The charger may be in one of several possible states. For example, it may be connected to one of the N buses, or it may be unconnected, giving a total of $N+1$ different states. This (time, state) 2-D representation is encoded as a rectangular grid of nodes. Node $n_{i,j}$ represents the charger in i^{th} state during the j^{th} time index (see figure 1). For example, $n_{1,0}$ from figure 1 represents a state where a charger is connected to Bus 1 at t_0.

We want the grid of nodes to encode the times at which each bus is at the station and available for charging. Therefore, let a nodes be present in the grid when the corresponding bus can connect to a charger, and delete from the grid nodes when a bus is away from the station. Consider the two bus scenario

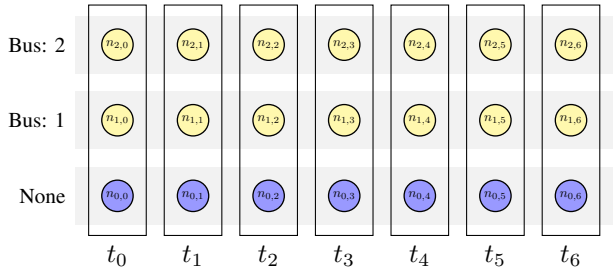

Fig. 1: Grid of nodes showing discrete timesteps advancing from left to right and charger states ascending vertically.

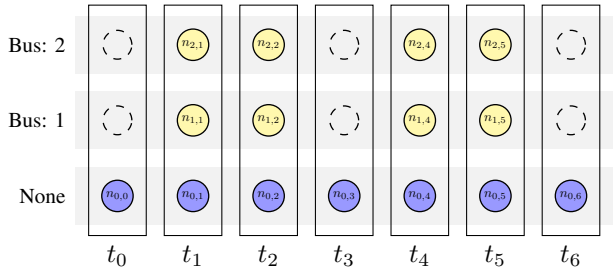

Fig. 2: Grid of nodes displaying times when buses are available for charging.

from figure 1 where buses 1 and 2 are away from the station at t_0, t_3, and t_6. The schedule is encoded by removing $n_{1,0}$, $n_{2,0}$, $n_{1,3}$, $n_{2,3}$, $n_{1,6}$, and $n_{2,6}$ to reflect the grid shown in figure 2.

The state of a charger at any time is represented by existing in a particular node. Changes in charger state over time are represented by the transitions from a node to multiple possible next nodes. These transitions are called edges (see figure 3) and represent four possible decisions: connect to a bus, charge a bus, remain idle, or disconnect from a bus. Edges are associated with actions and that action is determined by the nodes on either end. Consider the edge from $n_{0,0}$ to $n_{0,1}$ in figure 5. This edge represents a no-charge decision because the nodes on both ends represent the disconnected charge state at times t_0 and t_1. Chargers cannot charge while disconnected, so the edge decision is no-charge. Similarly, the edge between $n_{1,1}$ and $n_{1,2}$ indicates a decision to-charge as both $n_{1,1}$ and $n_{1,2}$ represent states where a charger is connected at times t_1 and t_2. Both to-charge and no-charge decisions are represented by *horizontal* transitions in the graph and only reflect the passing of time as no changes to the physical hardware are made.

Conversely, diagonal transitions imply physical hardware changes because they represent decisions where chargers connect to or disconnect from a bus. One such example from figure 5 includes the edge from $n_{0,0}$ to $n_{1,1}$. The state represented by $n_{0,0}$ is disconnected This edge represents an interval where a charger is disconnected at t_0 and connected at t_1, implying a 'to-connect' decision. The same logic applies in reverse for the edge between $n_{1,2}$ and $n_{0,3}$. Hence, the bus charge problem can be described in terms of nodes and edges (i.e. a graph) where nodes represent bus availability for charging and edges encode all possible charge decisions.

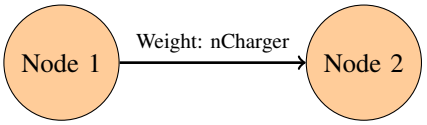

Fig. 3: Node to node connection.

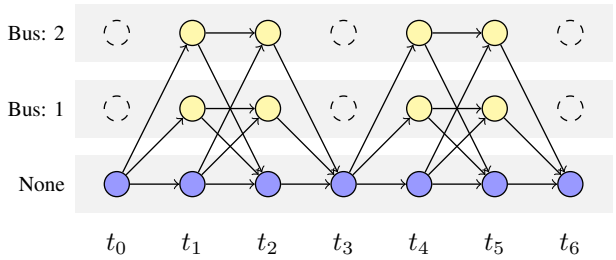

Fig. 4: Graph-based model of the complete decision-space.

A charge schedule can be thought of as a list of charge decisions that govern charge behavior. Because decisions are represented by edges in the graph, a schedule is also represented by a sequence of connected edges that form a path through the graph. If an edge is selected, or active, it is considered part of the path. Active and inactive edges are represented edge weights equal to 1 and 0, respectively.

A graph with binary edge weights can only represent a plan for one charger. This representation can be expanded to represent an arbitrary number of chargers by using integer valued weights, where each weight gives the number of chargers in the transition.

Consider a three-charger scenario using the graph in figure 4. A solution where one charger is connected to Bus 1 from t_1 to t_2 and to Bus 2 from t_4 to t_5 would be expressed by assigning unit weights to the appropriate connect, charge, and disconnect edges. The second charger remains idle as illustrated by the active edges along the bottom row of charger states (see figure 6).

In summary, the graph encodes bus availability with nodes, decisions with edges, and schedules with edge weights. Solv-

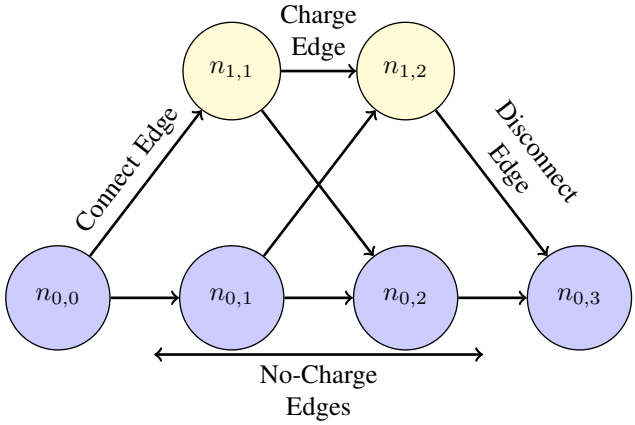

Fig. 5: Illustrates different types of edges: connect, disconnect, and charge edges.

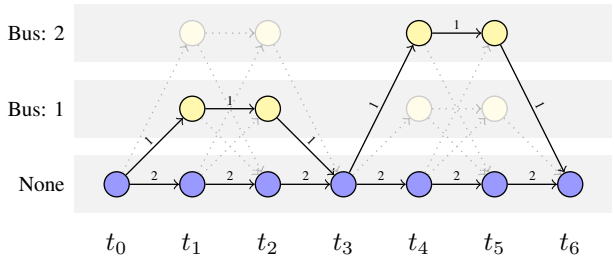

Fig. 6: A solution to a 2-bus 3-charger scenario.

ing the bus charge problem becomes a matter of finding the optimal set of edge weights, where optimal is meant to denote the most cost effective charge plan.

B. Graph Constraints

Finding the optimal charge schedule can be expressed as an optimization problem, where the graph is used to derive equality and inequality constraints for a mixed integer linear program (MILP)

$$\begin{aligned} &\min_{\mathbf{y}} \mathbf{r}^T\mathbf{y} \text{ subject to} \\ &F\mathbf{y} = \mathbf{f},\ Q\mathbf{y} \leq \mathbf{q}, \end{aligned} \tag{1}$$

where the equality and inequality constraints are encoded in F, $\mathbf{f}$, Q and $\mathbf{q}$. The variable $\mathbf{y}$ is a vector containing the elements of the solution and has the form

$$\mathbf{y} = \begin{bmatrix} \mathbf{x} \\ \mathbf{d} \\ \mathbf{g} \\ \mathbf{e} \\ \mathbf{p} \\ \hat{p} \\ \hat{p}_{\text{off-peak}} \\ \hat{p}_{\text{on-peak}} \end{bmatrix}, \tag{2}$$

where each element of $\mathbf{y}$ is defined later in this paper.

This subsection formulates two sets of constraints. The first represents the graph structure, enforces conservation of chargers, and defines the number of chargers through a set of net-flow constraints. The second prevents the charger from thrashing between connected/disconnected states and enforces one-bus/one-charger connectivity by enforcing what we call "group flow" constraints.

1) Net-Flow Constraints: Network flow constraints are expressed in matrix-vector form as

$$A\mathbf{x} = \mathbf{c}_f, \tag{3}$$

where A is the graph incidence matrix, $\mathbf{x}$ is the $n_E \times 1$ vector of edge weights and corresponds to $\mathbf{x}$ in equation 2, and $\mathbf{c}_f$ is $n_N \times 1$ and equals the difference between incoming and outgoing edge weights, or *net-flow*. The parameter n_E is the number of edges and n_N is the number of nodes.

An incidence matrix organizes relationships between nodes and edges by describing which edges leave and enter which nodes. The matrix A is an $n_N \times n_E$ matrix and expresses incoming connections between the i^{th} node and j^{th} edge by

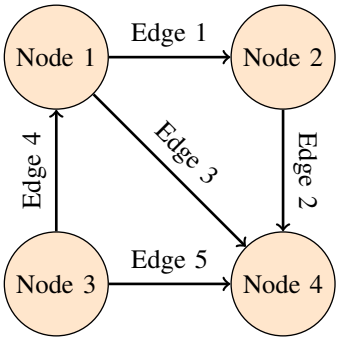

Fig. 7: A generic directed graph consisting of nodes and edges.

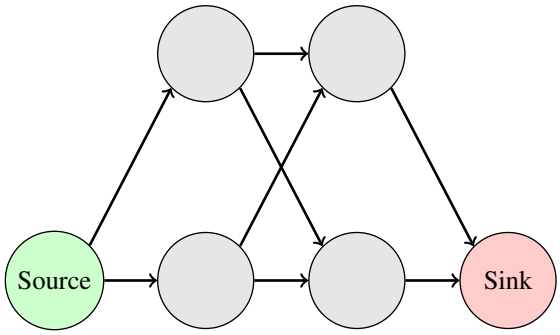

Fig. 8: Network flow illustrating sources and sinks.

$A_{i,j} = 1$. Similarly, outgoing connections are given by $A_{i,j} = -1$, and no connection with $A_{i,j} = 0$. For example, the graph in figure 7 is represented as:

$$\begin{bmatrix} -1 & 0 & -1 & 1 & 0 \\ 1 & -1 & 0 & 0 & 0 \\ 0 & 0 & 0 & -1 & -1 \\ 0 & 1 & 1 & 0 & 1 \end{bmatrix} \tag{4}$$

The difference between the number of chargers entering and leaving, or the *net-flow*, can be expressed in terms of A as seen in equation (3). Because the number of chargers does not change, the number of chargers entering and leaving a node must be equal. This is expressed in linear form as $a_i^T x = 0$, where a_i is the i^{th} row of A. The only exceptions occur at *source* and *sink* nodes.

A source node represents the beginning state for all chargers. Because edges originate here, there are no incoming edges and the net-flow will be minus the number of chargers. This is described in linear form as $a_i^T x = -n_C$, where n_C is the number of chargers.

Sink nodes represent the final state, where all edges terminate (see figure 8). Because sinks have no outgoing edges, they maintain a positive net-flow equal to the number of chargers and is expressed by $a_i^T = n_C$.

Therefore, the *flow constraints* require the elements of $\mathbf{c}_f$ be equal to zero for all non-source and non-sink nodes as seen in equation (5).

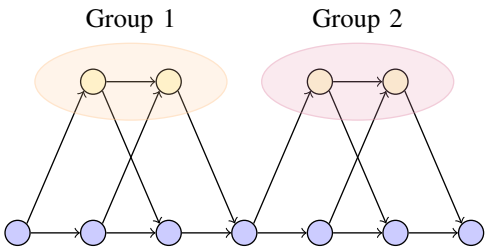

Fig. 9: Example of groups in a network flow graph.

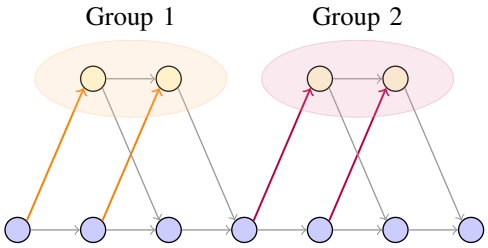

Fig. 10: Incoming group edges.

$$Ax = \begin{bmatrix} 0 \\ \vdots \\ -n_C \\ \vdots \\ 0 \\ n_C \\ \vdots \\ 0 \end{bmatrix}. \tag{5}$$

Equation 5 can be formulated in terms of $\mathbf{y}$ by appropriately zero-padding A such that

$$\begin{aligned} c_f &= \begin{bmatrix} A & 0 \end{bmatrix} \mathbf{y} \\ &= \tilde{A}\mathbf{y} \end{aligned} \tag{6}$$

2) Group-flow Constraints: Another flow type, known as group flow, can be used to regulate the number of chargers entering a set of nodes. This is desired for two reasons. First, it prevents chargers from connecting multiple times during an interval when a bus is available for charging, and it limits the number of chargers connecting to a bus to be one at most.

Define a charge group as the set of all nodes for a given bus corresponding to one station visit as shown in figure 9. The *group flow* is the number of chargers that enter a group and is represented as the sum of all incoming edge weights (see figure 10).

Denote the $n_G \times n_E$ group incidence matrix as B, where n_G is the number of groups and $B_{i,j}$ is 1 if the j^{th} edge enters the i^{th} group and 0 otherwise. For example, the group incidence matrix corresponding to the graph in figure 11 contains 1 in the 7^{th} and 10^{th} columns for Group 1, and the 12^{th} and 15^{th} columns for group 2 as given in equation 7.

$$B = \begin{bmatrix} 0\,0\,0\,0\,0\,0\,1\,0\,0\,1\,0\,0\,0\,0\,0\,0 \\ 0\,0\,0\,0\,0\,0\,0\,0\,0\,0\,0\,1\,0\,0\,1\,0 \end{bmatrix} \tag{7}$$

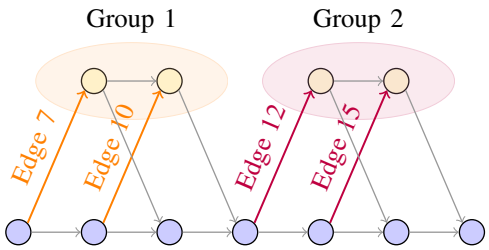

Fig. 11: Connect edge example for groups.

Let $\mathbf{x}$ be the edge weights as before and $\mathbf{c}_g$ be an $n_G \times 1$ vector where the i^{th} element gives the group flow for group i. The group flow is then computed as

$$B\mathbf{x} = \mathbf{c}_g \tag{8}$$

But the group flow is required to be one at most to avoid connection thrashing. This is expressed by the inequality given in equation (9).

$$Bx \leq \begin{bmatrix} 1 \\ 1 \\ \vdots \\ 1 \end{bmatrix}. \tag{9}$$

Similarly to (6), equation (9) can also be expressed in terms of $\mathbf{y}$ with appropriate zero padding as

$$\begin{aligned} \begin{bmatrix} B & 0 \end{bmatrix} \mathbf{y} &= \mathbf{1} \\ \tilde{B}\mathbf{y} &= \mathbf{1}. \end{aligned} \tag{10}$$

C. Section Summary

In summary, the bus charge problem can be formulated as a graph with nodes and edges, where charge plans are encoded as a path with unit edge weights. The charge problem aims to find a feasible path which minimizes the cost of power. Feasibility is defined through a set of net-flow and group-flow constraints. Net-flow constraints are encoded through an adjacency matrix and enforce both the conservation and total number of chargers. The group-flow constraints prevent connection thrashing and limit to one the number of simultaneous charger-to-bus connections.

IV. Battery State of Charge

Battery state of charge (SOC) plays a central role in the bus charge problem. Battery charge levels decay as a bus traverses a route. Solutions to the bus charge problem must account for bus routes and require that SOC values remain above a minimum threshold.

A SOC thresholding constraint requires that battery charge levels be modeled. The k^{th} SOC for bus i is denoted $d_{i,k}$, where k is the *node index*. The node indices used here are not directly tied to specific time steps. For example, $d_{i,k+1}$ represents the bus SOC at the node in the graph following the node where $d_{i,k}$ is the SOC as seen in figure 13. The set of all $d_{i,k}$ can be organized as the vector $\mathbf{d}$ from equation (2).

Because no charging is performed while on route, $d_{i,k}$ will assume its lowest value when buses enter the charge station.

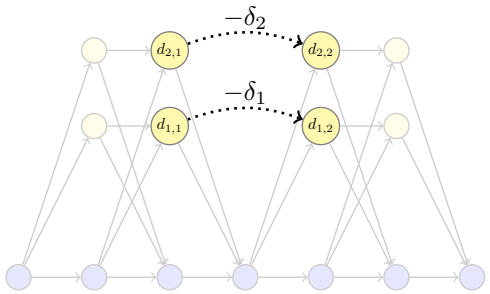

Fig. 12: Relationship between exit nodes (left) and entrance nodes (right) as δ

Let $d_{i,k+1}$ be the charge level for bus i as it enters the charge station, and δ_i represent the power discharged while on-route. The entrance SOC can be expressed as

$$d_{i,k+1} = d_{i,k} - \delta_i, \tag{11}$$

where $d_{i,k}$ is the previous departure SOC for bus i. Consider the example in figure 12, where buses 1 and 2 leave the station at t_2 and enter at t_4. The corresponding change in SOC is given as $d_{1,2} = d_{1,1} - \delta_1$ and $d_{2,2} = d_{2,1} - \delta_2$ for buses 1 and 2 respectively. The constraints from equation (11) can be expressed in linear standard form as

$$\begin{bmatrix} -1 & 1 \end{bmatrix} \begin{bmatrix} d_{i,k} \\ d_{i,k+1} \end{bmatrix} = \delta_i. \tag{12}$$

Equation (12) can be expressed in terms of $\mathbf{y}$ with appropriate zero padding and expanded to account for the decrease in SOC for all buses outside the station. The expanded constraint is given as

$$\begin{aligned} \begin{bmatrix} 0 & \dots & -1_{d_{i,k}} & 0 & \dots & 1_{d_{i,k+1}} \end{bmatrix} \mathbf{y} &= \mathbf{d}_\delta \\ D_\delta \mathbf{y} &= \mathbf{d}_\delta, \end{aligned} \tag{13}$$

where $-1_{d_{i,k}}$ and $1_{d_{i,k+1}}$ represent -1 and 1 in locations corresponding to $d_{i,k}$ and $d_{i,k+1}$ respectively. Similar notation will be used throughout this paper as a means to imply a corresponding index for other variables.

Time periods between entrance and exit nodes represent time spent in the charge station and have the potential to charge the battery. An edge over which charging occurs is referred to as $x_{i,k}$, where k gives the index of the edge's outgoing node, and i refers to the bus. When a charger occupies $x_{i,k}$, the resulting increase, or *gain*, in battery charge is denoted $g_{i,k}$, where i and k mirror the edge indices (see figure 13).

The value for $g_{i,k}$ is computed using a single charge rate. Multiple charge rates can be encoded by connecting bus nodes with multiple edges, denoted $x_{i,k,l}$, where each edge has a distinct charge rate and gain denoted $g_{i,k,l}$ (see figure 14). Having multiple charge rates gives the option for fast charging when necessary, and slow charging when possible to preserve battery health and decrease the electrical load [9].

The rate is selected by setting $x_{i,k,l} = 1$. All gains associated with unselected rates are set to zero. Gains that correspond to selected rates are computed using the constant

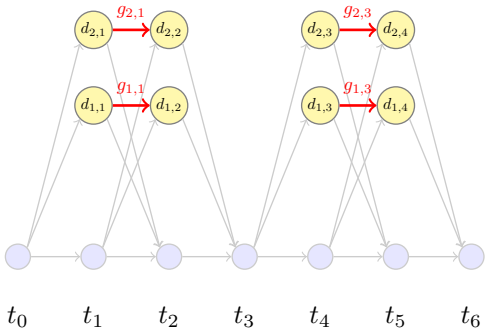

Fig. 13: Depiction of which edges increase SOC for the single rate case

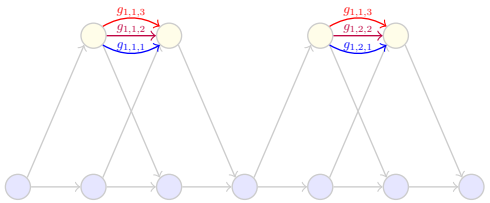

Fig. 14: Multi-Rate Charging

current constant voltage (CCCV) model as derived in [19] which gives:

$$d_{i,k+1} = \bar{a}_l d_{i,k} - \bar{b}_l M, \tag{14}$$

where $\bar{a}_l \sim (0, 1]$, depends on the charge rate and is experimentally determined, M is the battery capacity in kWh, and $\bar{b}_l = \bar{a}_l - 1$. Equation (14) is used to show that

$$\begin{aligned} d_{i,k+1} &= \bar{a}_l d_{i,k} - \bar{b}_l M \\ d_{i,k+1} - d_{i,k} &= \bar{a}_l d_{i,k} - \bar{b}_l M - d_{i,k}, \end{aligned} \tag{15}$$

but the gain is equal to the difference in $d_{i,k+1}$ and $d_{i,k}$ such that $g_{i,k,l} = d_{i,k+1} - d_{i,k}$. So

$$\begin{aligned} g_{i,k,l} &= \bar{a}_l d_{i,k} - \bar{b}_l M - d_{i,k} \\ g_{i,k,l} &= (\bar{a}_l - 1) d_{i,k} - \bar{b}_l M. \end{aligned} \tag{16}$$

Therefore,

$$\begin{cases} g_{i,k,l} = d_{i,k}(\bar{a}_l - 1) - \bar{b}_l M & x_{i,k,l} = 1 \\ g_{i,k,l} = 0 & x_{i,k,l} = 0 \end{cases}. \tag{17}$$

The conditions given in equation 17 can be rewritten as

$$\begin{aligned} &\begin{cases} g_{i,k,l} \le d_{i,k}(\bar{a}_l - 1) - \bar{b}_l M \\ g_{i,k,l} \ge d_{i,k}(\bar{a}_l - 1) - \bar{b}_l M & x_{i,k,l} = 1 \\ g_{i,k,l} \le 0 \\ g_{i,k,l} \ge 0 & x_{i,k,l} = 0 \end{cases} \\ \Rightarrow\ &\begin{aligned} &g_{i,k,l} \le d_{i,k}(\bar{a}_l - 1) - \bar{b} M - M(1 - x_{i,k,l}) \\ &g_{i,k,l} \ge d_{i,k}(\bar{a}_l - 1) - \bar{b} M \\ &g_{i,k,l} \le 0 + M x_{i,k,l} \\ &g_{i,k,l} \ge 0, \end{aligned} \end{aligned} \tag{18}$$

where M is the battery capacity. The results of equation 18 obtain a switching effect. When $x_{i,k,l} = 1$, equation 18 becomes

$$\left.\begin{aligned} g_{i,k,l} &\leq d_{i,k}(\bar{a}_l - 1) - \bar{b}_l M \\ g_{i,k,l} &\geq d_{i,k}(\bar{a}_l - 1) - \bar{b}_l M \end{aligned}\right\} \text{Active}$$
$$\left.\begin{aligned} g_{i,k,l} &\leq M \\ g_{i,k,l} &\geq 0 \end{aligned}\right\} \text{Inactive} \tag{19}$$

The active constraints imply equality for $g_{i,k,l} = (\bar{a}_l - 1)d_{i,k} - \bar{b}_l M$. The inactive constraints imply that $g_{i,k,l}$ is greater than zero and less than the battery capacity, which are trivially satisfied. When $x_{i,k,l} = 0$, equation 18 becomes

$$\left.\begin{aligned} g_{i,k,l} &\leq d_{i,k}(\bar{a}_l - 1) - \bar{b}_l M - M \\ g_{i,k,l} &\geq d_{i,k}(\bar{a}_l - 1) - \bar{b}_l M \end{aligned}\right\} \text{Inactive}$$
$$\left.\begin{aligned} g_{i,k,l} &\leq 0 \\ g_{i,k,l} &\geq 0 \end{aligned}\right\} \text{Active} \tag{20}$$

where the inactive constraints are again trivially satisfied, and the active constraints imply equality for $g_{i,k,l} = 0$.

Equation (18) can be expressed in standard form as

$$\begin{aligned} -g_{i,k,l} + d_{i,k}(\bar{a}_l - 1) + x_{i,k,l} &\leq M(\bar{b}_l + 1) \\ g_{i,k,l} - d_{i,k}(\bar{a}_l - 1) &\leq -\bar{b}_l M \\ g_{i,k,l} - M x_{i,k,l} &\leq 0 \\ -g_{i,k,l} &\leq 0 \end{aligned} \tag{21}$$

and in matrix form as

$$\begin{bmatrix} -1 & \bar{a}_l - 1 & 1 \\ 1 & 1 - \bar{a}_1 & 0 \\ 1 & 0 & -M \\ -1 & 0 & 0 \end{bmatrix} \begin{bmatrix} g_{i,k,l} \\ d_{i,k} \\ x_{i,k,l} \end{bmatrix} \leq \begin{bmatrix} M(\bar{b}_l + 1 \\ -\bar{b}_l M \\ 0 \\ 0 \end{bmatrix}. \tag{22}$$

Equation (22) can be expanded to include constraints for all $g_{i,k,l}$. Because each value for $g_{i,k,l}$, $d_{i,k}$, and $x_{i,k,l}$ is an element of $\mathbf{y}$, the constraints from equation 22 can be written as

$$G\mathbf{y} \leq \mathbf{b}_g. \tag{23}$$

The value of $d_{i,k}$ can be expressed as

$$d_{i,k+1} = d_{i,k} + \sum_l g_{i,k,l} \tag{24}$$

or

$$d_{i,k+1} - d_{i,k} - \sum_l g_{i,k,l} = 0 \tag{25}$$

because a non-zero element of $g_{i,k,l}$ is only present for one corresponding l. This relationship is described in terms of an equality constraint such that

$$\begin{bmatrix} 1 & -1 & \dots & -1 \end{bmatrix} \begin{bmatrix} d_{i,k+1} \\ d_{i,k} \\ g_{i,k,1} \\ \dots \\ g_{i,k,l} \end{bmatrix} = 0. \tag{26}$$

Equation (26) can be appropriately zero padded to give

$$\begin{bmatrix} 1_{d_{i,k+1}} & -1_{d_{i,k}} & \dots & -1_{g_{i,k,l}} \end{bmatrix} \mathbf{y} = 0. \tag{27}$$

and expanded to define the values for all $d_{i,k} \ni k > 0$ as

$$D_d \mathbf{y} = \mathbf{0}. \tag{28}$$

The values for $d_{i,0}$ are defined with initial SOC conditions with additional equality constraints, denoted $\mathbf{d}_0$ such that

$$\begin{bmatrix} 1_{d_{1,0}} & 0 & 0 & \dots & 0 \\ 0 & \dots & 1_{d_{2,0}} & 0 & 0 \\ \vdots & & \vdots & & \vdots \\ 0 & 0 & 0 & \dots & 1_{d_{i,0}} \end{bmatrix} \mathbf{y} = \mathbf{d}_0, \tag{29}$$

or

$$D_0 \mathbf{y} = \mathbf{d}_0. \tag{30}$$

Once all values for $d_{i,k}$ are computed, they must be constrained to remain above a threshold τ. The SOC thresholding constraint can be expressed as an inequality constraint such that

$$\begin{aligned} & d_{i,k} \geq \tau \\ \Rightarrow & -d_{i,k} \leq -\tau \\ \Rightarrow & \begin{bmatrix} 0 & \dots & -1_{d_{i,k}} & \dots & 0 \end{bmatrix} \mathbf{y} \leq -\tau \end{aligned} \tag{31}$$

Equation (31) can be expanded to a matrix D_τ, where each $d_{i,k}$ contains a corresponding constraint row such that

$$\begin{aligned} D_\tau \mathbf{y} &\leq \begin{bmatrix} -\tau \\ \vdots \\ -\tau \end{bmatrix} \\ &\leq \mathbf{d}_\tau \end{aligned} \tag{32}$$

In summary, the minimum SOC for all feasible charge plans must exceed a given threshold. SOC values are computed while the bus is in the charge station. SOC values are updated when a bus enters by subtracting the discharged energy from the previous SOC estimate. SOC values are updated for in-station periods by adding the charge gains as given in equation (24). Gains are computed using a switching constraint which sets them to zero when not charging, otherwise they follow the CCCV model as set forth in equation (16). Initial SOC values are handled with the equality constraint given in equation (30) and the SOC is constrained to remain above the threshold τ in equation (32). All constraints for d can be concatenated such that

$$\begin{bmatrix} D_0 \\ D_\delta \\ D_d \end{bmatrix} \mathbf{y} = \begin{bmatrix} \mathbf{d}_0 \\ \mathbf{d}_\delta \\ \mathbf{0} \end{bmatrix}, \quad \begin{bmatrix} D_g \\ D_\tau \end{bmatrix} \mathbf{y} \leq \begin{bmatrix} \mathbf{d}_g \\ \mathbf{d}_\tau \end{bmatrix} \tag{33}$$

and expressed as

$$D_{\text{eq}} \mathbf{y} = \mathbf{d}_{\text{eq}}, \quad D_{\text{ineq}} \mathbf{y} \leq \mathbf{d}_{\text{ineq}}. \tag{34}$$

V. Multi-Graph Additions

An additional contribution this work offers is the expansion to joint optimization of both night and day charging in a single optimization problem. Day and night operations differ in two aspects: number of chargers and bus availability. During the day, the buses can charge only at the charge station. The number of chargers in the station are limited, causing contention between buses. At night, each bus docks in a

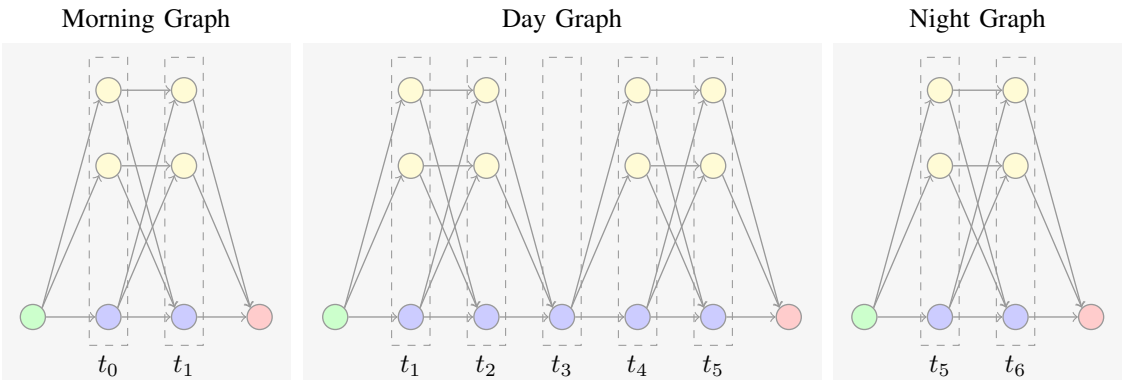

Fig. 15: Night and day graphs.

holding stall with one charger per stall, eliminating charger contention. Furthermore, nighttime charging is slow compred to daytime charing. Our model uses different rates for day and night charging.

Bus availability also changes because buses do not leave their stalls at night. This simplifies the charge problem because buses are always available for charging.

Equation (5) in section III-B1 describes the net-flow constraints which constrain the number of chargers in the source and sink nodes. Because the number of chargers are different from night to day, a separate graph is used at each transition as shown in figure 15.

Each graph is connected by equating the appropriate SOC values. Consider the multi-graph formulation given in figure 16. The morning graph is related to the day graph because $d_{1,1}$ and $d_{2,1}$ represent the same SOC values as $d_{1,2}$ and $d_{2,2}$ respectively. The same applies for the day and night graphs, where $d_{1,5}$ and $d_{2,5}$ represent the SOC values for $d_{1,6}$ and $d_{2,6}$. This equality relationship can be expressed as an equality constraint where

$$\mathbf{d}_{\text{graph 1}} - \mathbf{d}_{\text{graph 2}} = \mathbf{0} \tag{35}$$

or by

$$D_{\text{multi-graph}}\mathbf{y} = \mathbf{0}, \tag{36}$$

where $D_{\text{multi-graph}}$ is an nBus $\times$ nVar matrix such that

$$D_{\text{multi-graph}}\mathbf{y} = \mathbf{d}_{\text{graph 1}} - \mathbf{d}_{\text{graph 2}}. \tag{37}$$

Because all SOC values d are contained in $\mathbf{y}$, forming the matrix D amounts to placing 1 and -1 at the indices corresponding to $d_{\text{graph 1}}$ and $d_{\text{graph 2}}$ respectively and zero otherwise.

VI. Objective Function

The objective function in this work models the rate schedule used in [16], where the cost is modeled as the monthly charge a transit authority receives from the power provider. The objective function includes charges for energy, power, and facility use and implements both on and off-peak rates.

The objective function also includes effects and costs of uncontrolled loads. Uncontrolled loads might include the effects of patrons charging personal electric vehicles, electric trains passing through, CNG stations, etc. The loads used in this work were recorded at the UTA Intermodal Hub station in Salt Lake City (SLC), Utah as the average power sampled at uniform time intervals.

A. Energy

Energy cost is assessed per Kilowatt-hour of energy consumed and includes energy consumed by uncontrolled loads and bus chargers. Let $\mathbf{p}$ be the average external power used at each timestep, where $\mathbf{p}_i$ is the average power draw between t_j and t_{j+1}. The energy consumed by external loads from t_j to t_{j+1} is computed as

$$e_j^l = \mathbf{p}_i \cdot \Delta_t, \tag{38}$$

where Δ_t is the change in time from t_j to t_{j+1} in hours. The energy consumed by bus chargers for the same interval is computed as

$$e_j^b = \sum_{k \in t} g_{i,k,l}, \tag{39}$$

where $k \in t$ represents all values for g that took place between t_i and t_{i+1}. The total energy is computed as

$$e_j = e_j^l + e_j^b \tag{40}$$

Equation (40) can be written in standard form as

$$\begin{gathered} e_j - \sum_{k \in t} g_{i,k,l} = p_i \cdot \Delta_t \\ \begin{bmatrix} 1_{e_j} & -1_{g_1} & \dots & -1_{g_n} \end{bmatrix} \begin{bmatrix} e_j \\ g_1 \\ \vdots \\ g_n \end{bmatrix} = p_i \cdot \Delta_t \end{gathered} . \tag{41}$$

Because power providers charge different rates for the total power consumed during the respective on and off-peak hours, equation (41) be modified to reflect the energy consumed in arbitrary time periods. Let T be a set of t_j, or just j, which will later be used to denote on and off-peak periods as T_{on}

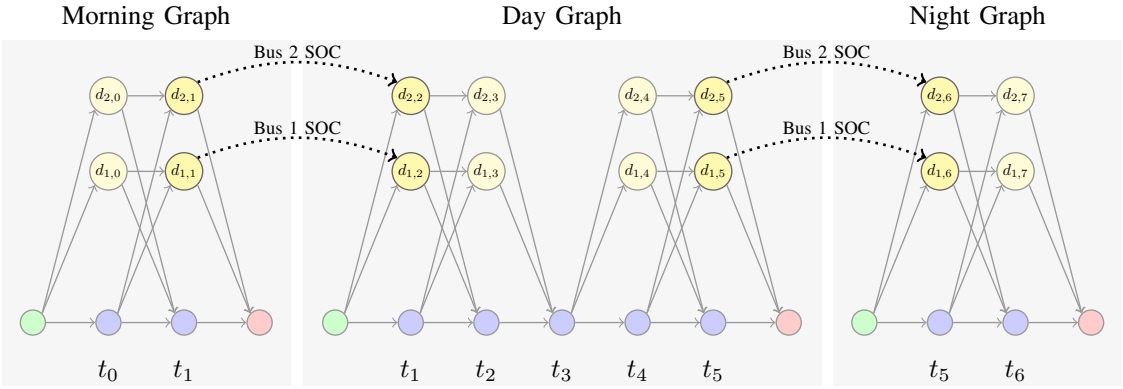

Fig. 16: Bus SOC between night and day graphs.

and T_{off}. Equation 41 can be expanded to compute the total energy consumed in T as

$$\begin{aligned} e_T - \sum_{k \in T} g_{j,k,l} &= \left(\sum_{j \in T} p_j \right) \cdot \Delta_t \\ \begin{bmatrix} 1_{e_T} & -1_{g_1} & \dots - 1_{g_n} \end{bmatrix} \begin{bmatrix} e_T \\ g_1 \\ \vdots \\ g_n \end{bmatrix} &= e_T^{\text{load}} \end{aligned} \tag{42}$$

For multiple time periods, the constraint can be expanded in matrix form, where row i corresponds to the periods of time in T_i. Furthermore, by including the values for each e_{T_i} in $\mathbf{y}$ and zero-padding appropriately, the expanded form of equation (42) can be written as

$$E\mathbf{y} = \mathbf{e}^{\text{load}}, \tag{43}$$

where row i in E reflects equation (42) for the time intervals in T_i, and $\mathbf{e}_i^{\text{load}}$ contains the energy consumed by uncontrolled loads during T_i.

B. Power

Power costs are computed for the maximum average power draw, where the average is computed over a 15 minute sliding window. The average power can be computed as the energy in the window divided by the window length in hours. In this case, a 15 minute window equates to a quarter hour. Let $\bar{p}_j$ be the average power from $j-15$ to j. Equation (42) can be adapted to compute the average power as

$$\begin{aligned} \bar{p}_j - \left(\sum_{k \in T_j} \frac{1}{4} g_{i,k,l} \right) &= \left(\sum_{i \in T_j} p_i \right) \cdot \frac{\Delta_t}{4} \\ \begin{bmatrix} 1_{\bar{p}_j} & -\frac{1_{g_1}}{4} & \dots - \frac{1_{g_n}}{4} \end{bmatrix} \begin{bmatrix} e_j \\ g_1 \\ \vdots \\ g_n \end{bmatrix} &= \frac{p_T \cdot \Delta_t}{4}. \end{aligned} \tag{44}$$

Equation (44) can further be expanded and zero padded to compute the average power at each time, t_j by applying equation (44) to the corresponding window as

$$P\mathbf{y} = \mathbf{p}. \tag{45}$$

The maximum average power, denoted $\hat{p}$, is greater than or equal to each average power computed in equation (45). This yields an additional set of inequality constraints

$$\begin{aligned} \begin{bmatrix} -1_{\hat{p}} & 1_{\bar{p}_0} & 0 & \dots & 0 \\ -1_{\hat{p}} & 0 & 1_{\bar{p}_1} & \dots & 0 \\ -1_{\hat{p}} & 0 & 0 & \dots & 1_{\bar{p}_j} \end{bmatrix} \mathbf{y} &\leq \mathbf{0} \\ P_{\text{max}}\mathbf{y} &\leq \mathbf{0}. \end{aligned} \tag{46}$$

Because the max average power is minimized in the objective function, the value for $\hat{p}_{\text{max}}$ will be forced down to the value of the greatest average power computed in equation (45), and accurately reflect the maximum average power.

C. On/Off Peak Rates

Power providers divide each day into on and off-peak periods during which different rates are applied for both energy and power costs. Let H and L be the respective sets of all time indices in on and off peak periods respectively. The cost of energy during on-peak hours can be expressed as

$$\begin{aligned} c_{\text{energy}_H} &= \left(\sum_{j \in H} e_j \right) r_{e_{\text{on}}} \\ &= \begin{bmatrix} r_{e_1} & 0 & \dots & 0 & r_{e_4} & \dots & 0 \end{bmatrix} \mathbf{y} \\ &= \mathbf{r}_{e_{\text{on}}}^T \mathbf{y}, \end{aligned} \tag{47}$$

where $\mathbf{r}_e^{\text{on}}$ contains the value of r_e^{on} at the index corresponding to e_j in $\mathbf{y}$ $\forall j \in H$. A similar formulation can be used to describe the cost of energy consumed during off-peak hours.

An on-peak rate also applies to charges for power. Equation (46) can be adapted to only include rows that correspond to average power values during on-peak hours such that

$$\begin{aligned} \begin{bmatrix} -1_{\hat{p}_{\text{on}}} & 1_{\bar{p}_0} & 0 & \dots & 0 \\ -1_{\hat{p}_{\text{on}}} & 0 & 1_{\bar{p}_1} & \dots & 0 \\ -1_{\hat{p}_{\text{on}}} & 0 & 0 & \dots & 1_{\bar{p}_j} \end{bmatrix} \mathbf{y} &\leq \mathbf{0} \\ P_{\text{on}}\mathbf{y} &\leq \mathbf{0}. \end{aligned} \tag{48}$$

Similarly, the off-peak max average power can be computed as

$$\begin{aligned} \begin{bmatrix} -1_{\hat{p}_{\text{off}}} & 1_{\bar{p}_0} & 0 & \dots & 0 \\ -1_{\hat{p}_{\text{off}}} & 0 & 1_{\bar{p}_1} & \dots & 0 \\ -1_{\hat{p}_{\text{off}}} & 0 & 0 & \dots & 1_{\bar{p}_j} \end{bmatrix} \mathbf{y} &\leq \mathbf{0} \\ P_{\text{off}}\mathbf{y} &\leq \mathbf{0}, \end{aligned} \tag{49}$$

where each row corresponds to $\bar{p}_j \ \forall j \in L$.

Many power providers include a facilities charge. The facilities charge is assessed per kW of the maximum average power and ignores on and off-peak times. The total max average power is calculated using equation (46).

The total power cost can be computed as the sum of the on-peak, off-peak, and facilities charges as

$$\begin{aligned} c_{\text{power}} &= \begin{bmatrix} r_{\hat{p}_{\text{on}}} & 0 & \dots & 0 & r_{\hat{p}_{\text{off}}} & 0 & \dots & 0 & r_{\hat{p}_{\text{facilities}}} \end{bmatrix} \mathbf{y} \\ &= \mathbf{r}_{\hat{p}}^T \mathbf{y} \end{aligned} \tag{50}$$

D. Objective Function

The objective function combines the cost of energy and power, where the on-peak and off-peak energy is combined as

$$\begin{aligned} c_{\text{energy}} &= \mathbf{r}_{e_{\text{on}}}^T \mathbf{y} + \mathbf{r}_{e_{\text{off}}}^T \mathbf{y} \\ &= \left(\mathbf{r}_{e_{\text{on}}} + \mathbf{r}_{e_{\text{off}}}\right)^T \mathbf{y} \\ &= \mathbf{r}_e^T \mathbf{y}. \end{aligned} \tag{51}$$

The combined expression is given as

$$\begin{aligned} c_{\text{total}} &= c_{\text{power}} + c_{\text{energy}} \\ &= \mathbf{r}_e^T \mathbf{y} + \mathbf{r}_{\hat{p}}^T \mathbf{y} \\ &= \left(\mathbf{r}_e + \mathbf{r}_{\hat{p}}\right)^T \mathbf{y} \\ &= \mathbf{r}^T \mathbf{y}. \end{aligned} \tag{52}$$

Equation (52) is used as the objective function in a mixed integer linear program of the form

$$\begin{aligned} &\min_{\mathbf{y}} \ \mathbf{r}^T \mathbf{y} \text{ subject to} \\ &C_{\text{eq}} \mathbf{y} = \mathbf{c}_{\text{eq}}, \ C_{\text{ineq}} \mathbf{y} \leq \mathbf{c}_{\text{ineq}}, \end{aligned} \tag{53}$$

where $C_{\text{eq}}, \mathbf{c}_{\text{eq}}, C_{\text{ineq}}$, and $\mathbf{c}_{\text{ineq}}$ are formed by stacking the equality and inequality constraints from equations (6), (10), (34), (45), (46), (48), and (49),

$$\min_{\mathbf{y}} \ \mathbf{r}^T \mathbf{y} \text{ subject to}$$
$$\begin{bmatrix} \tilde{A} \\ D_{\text{eq}} \\ P \end{bmatrix} \mathbf{y} = \begin{bmatrix} \mathbf{c}_f \\ \mathbf{d}_{\text{eq}} \\ \mathbf{p} \end{bmatrix}, \ \begin{bmatrix} \tilde{B} \\ D_{\text{ineq}} \\ P_{\max} \\ P_{\text{on}} \\ P_{\text{off}} \end{bmatrix} \mathbf{y} \leq \begin{bmatrix} \mathbf{1} \\ \mathbf{d}_{\text{ineq}} \\ \mathbf{0} \\ \mathbf{0} \\ \mathbf{0} \end{bmatrix}. \tag{54}$$

VII. Results

This section contains results of the planning framework and is subdivided into three subsections: uncontested results, contested results, and multi-rate comparisons.

A. Baseline and Setup

The experiments in this section compare the results of the framework given in equation (54) with a baseline, which models the general behavior of bus drivers at the Utah Transit Authority (UTA) in SLC, Utah. According to UTA, bus drivers usually charge whenever possible. As they enter the station, the bus drivers look to see if an overhead charger is available. If so, they stop there, plug in, and top off their bus's battery. Our baseline scenario reflects this default bus driver behavior using an objective function that maximizes the number of charging instances, which is computed as the sum of group flow values, resulting in the objective function

$$\max_{\mathbf{y}} \ \mathbf{1}^T B \mathbf{y}, \tag{55}$$

All other constraints are the same, which results in the baseline formulation

$$\max_{\mathbf{y}} \ \mathbf{1}^T B \mathbf{y} \text{ subject to}$$
$$\begin{bmatrix} \tilde{A} \\ D_{\text{eq}} \\ P \end{bmatrix} \mathbf{y} = \begin{bmatrix} \mathbf{c}_f \\ \mathbf{d}_{\text{eq}} \\ \mathbf{p} \end{bmatrix}, \ \begin{bmatrix} \tilde{B} \\ D_{\text{ineq}} \\ P_{\max} \\ P_{\text{on}} \\ P_{\text{off}} \end{bmatrix} \mathbf{y} \leq \begin{bmatrix} \mathbf{1} \\ \mathbf{d}_{\text{ineq}} \\ \mathbf{0} \\ \mathbf{0} \\ \mathbf{0} \end{bmatrix}. \tag{56}$$

Each experiment is run using a five minute timestep such that the time difference between t_k and t_{k+1} is five minutes. Four charge rates are used during the following experiments: $\bar{a}_1 = 0.9851$, $\bar{a}_2 = 0.9418$, $\bar{a}_3 = 0.9003$, and $\bar{a}_4 = 0.8607$. Each value for $\bar{a}$ represents a different charge rate and is referenced by how much time it would take a bus to charge from 0% to 99%. For the rates used in the following set of experiments, a bus would need 25.58 hours to charge from 0% to 99% with $\bar{a}_1$, 6.4 hours with $\bar{a}_2$, 3.65 with $\bar{a}_3$, and 2.56 with $\bar{a}_4$.

Night charging uses a single charge rate of $\bar{a}_1$ for all experiments. Experiments with single rate day charging use $\bar{a}_4$, and multi-rate experiments incorporate four charge options: $\bar{a}_1$, $\bar{a}_2$, $\bar{a}_3$, and $\bar{a}_4$.

Uncontrolled loads are modeled with data from the TRAX Power Substation (TPSS) at the UTA Intermodel Hub site in Salt Lake City. It is also assumed that each bus starts and ends each day with an SOC of 80% and has a maximum charge capacity of 100 kWh.

B. Uncontested Results

This section explores performance in a scenario where there is one charger per bus during the day, making charge resources *uncontested*. The optimal charge schedule associated with equation 54 is compared with the schedule developed by the baseline in equation (56). The total monthly cost is computed using the rates given in Rocky Mountain Power Schedule 8 and is computed in equation (57).

$$\begin{aligned} \text{cost} = \ &\text{facilitiesPower} \cdot 4.81 + \text{onPeakPower} \cdot 15.73 + \\ &\text{onPeakEnergy} \cdot 0.058282 + \text{offPeakEnergy} \cdot 0.029624 \end{aligned} \tag{57}$$

There is also a customer service charge of 71.00 in the rate schedule, but because the service charge does not depend on a customer's behavior, it is ignored.

Because equation (57) is driven by facilities power, on-peak power, on-peak energy, and off-peak energy, these four criteria are used to evaluate the optimal and baseline charge plans. Furthermore, because the on and off-peak energy charges contribute little to the cost differences, they have been grouped together for comparison.

Figure 17 compares the cost of energy, on-peak power, and facilities power. Note how the energy costs are essentially

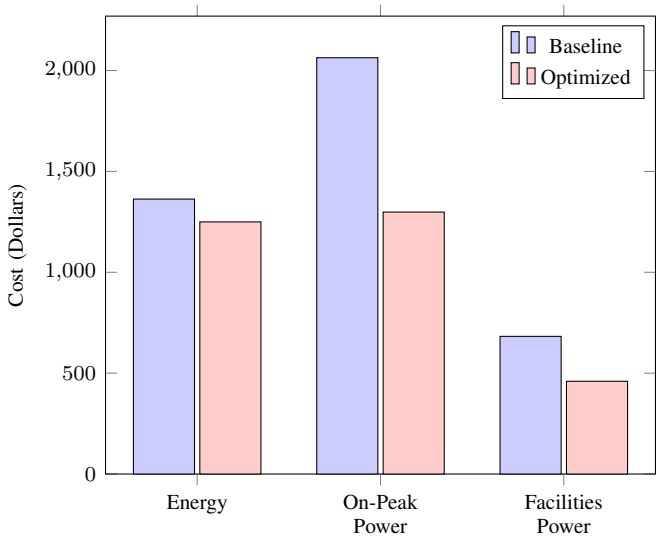

Fig. 17: Cost comparison between optimized and baseline algorithms.

equal, which indicates that similar amounts of energy were consumed in both scenarios. The facilities and on-peak power costs, however are significantly larger for the baseline schedule. To better understand the cost disparity, we observe the load profiles to identify how the optimized schedule avoids the costs incurred by the baseline.

Figure 18 shows the 15 minute average power for both the baseline and optimal schedules. Note how the optimal schedule incurs a lower average power for both on and off peak time intervals. The reduction in average power is what lead to the cost disparity between the on-peak and facilities power costs in figure 17.

The underlying behavior can be observed in figure 19, which separates the loads into their controlled and uncontrolled constituents. Because the uncontrolled loads are shared between both scenarios, figure 19 shows the 15 minute average power for uncontrolled, optimal charging, and baseline charging loads.

Observe how the optimized schedule avoids charging during on-peak hours and regulates each charge event to spread the power draw over larger periods of time. Furthermore, bus charging is avoided when uncontrolled loads are high, resulting in a reduced 15 minute average power. Reducing the average power and not charging during on-peak periods results in the dramatic cost reduction shown in figure 17.

C. Contested Results

This section observes the performance of the optimal schedule as charge resources become scarce, creating a contested environment. Resource contention is most prevalent when chargers are scarce and pushes buses to charge in non-ideal circumstances. For example, if charging resources are saturated during off-peak hours, other buses might be forced to charge in the on-peak window. The impact of contention is measured as the change in monthly cost when the number of chargers is held constant and the number of buses increases.

In this analysis, one charger is used and the number of buses is varied from five to eleven. Figure 20 shows the monthly cost as a function of the number of buses. Note the minimal cost increase per bus, where each successive bus costs around $\$75.00$, which approaches the cost of energy that is required to provide transit services. Because the additional cost per bus is roughly the cost of energy, there are no additional facilities and on-peak power charges, showing that optimal charge plans also minimize cost in the presence of contention.

We desire to know how this is achieved. Figure 21 shows the 15-minute average power for controlled and uncontrolled loads for a five bus and eleven bus scenario. In the 5 bus scenario, loads are easily distributed amongst off-peak hours, resulting in an optimized cost. The 11 bus scenario requires significantly more power and is forced to charge during on-peak hours. Note however that the average power is kept relatively low, and the additional charge sessions never cause the average power to supersede the maximum average power of the uncontrolled loads. Both scenarios also make ample use of night charging, where the number of chargers is the same as the number of buses.

D. Multi-Rate Comparison

This subsection compares a multi-rate and single-rate charge schedule. The multi-rate schedule includes a_1, a_2, a_3, and a_4 as defined in section VII-A. The single-rate schedule assumes the static charge rate associated with a_1. Two scenarios are considered. The first compares the cost of mulit and single-rate plans for a 5 bus 1 charger scenario. The second compares performance for a 35 bus, 6 charger scenario.

The respective costs assocaited with the 5 bus 1 charger scenario are given in figure 22 as before. As shown in figure 22, the cost difference is negligible. The cost of the multi-rate scenario is \$3006.94 and the cost of the single-rate scenario is \$3007.77 which gives a total savings of \$0.83. The 36 bus, 6 charger comparison in figure 23 also yields minimal cost savings.

While examining the most commonly used edges, we observe that edges corresponding to a maximum charge rate are used most frequently as shown in figure 24 which explains the similarities in cost. If the highest rate is almost always selected, the resulting plan would resemble a single-rate schedule, resulting in a singe-rate cost.

Another explaination for the cost similarity is found in how monthly cost is computed. Because the monthly cost is based on the average instantanous power, both high and low charge rates can give the same results over a fixed time period. The charge schedules shown in both single and multi-rate plans charge buses in relatively small time periods. Fast charging over small periods of time is equivalent to slow charging over longer periods. In this way, the average power can be kept low even when using high charge rates (see figures 21 and 20).

VIII. Conclusions and Future Work

In conclusion, the charge schedules developed in equation (54) yield significant cost savings over the baseline case.

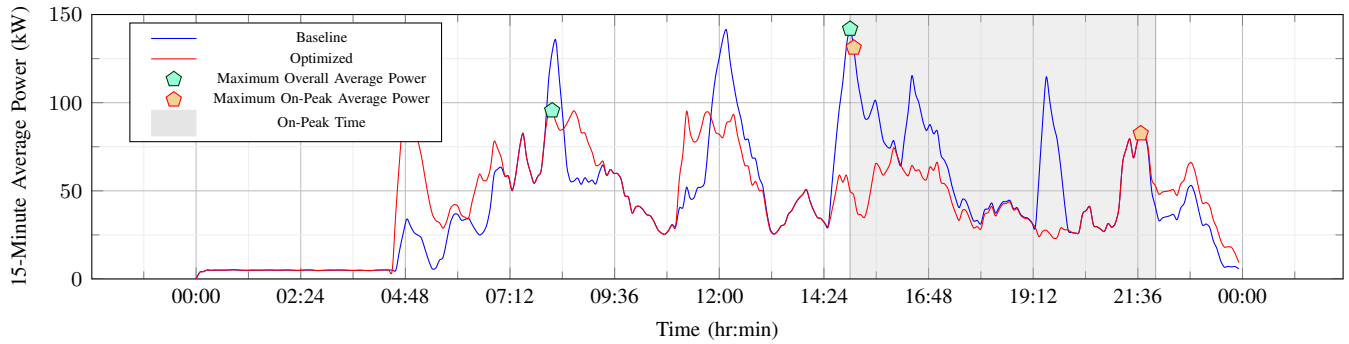

Fig. 18: 15-Minute average power for one day.

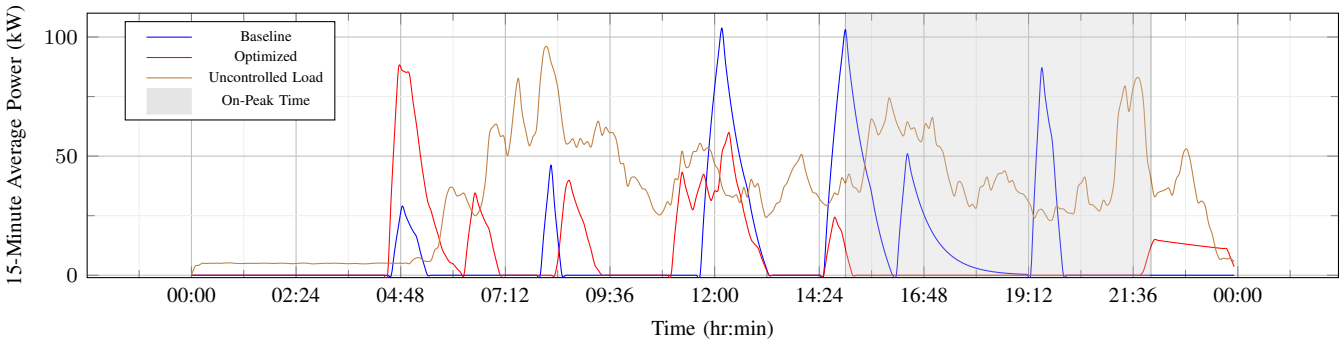

Fig. 19: Comparison between uncontrolled and bus loads.

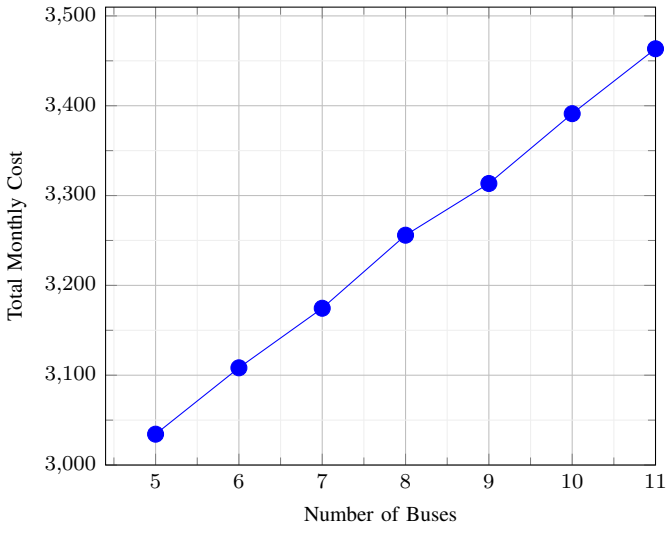

Fig. 20: Results for several single charger scenarios.

These savings come from minimizing the average power consumption, and charging during off-peak hours. Cost savings are maintained in both uncontested and resource constrained scenarios. There is also little to be gained by offering multiple charge rates because average power can be managed with high charge rates by reducing the charge duration. Furthermore, it was shown that when given the choice, the optimizer primarily selected high charge rates, which reduces the problem complexity to the single-rate formulation.

Although multi-rate charging does not significantly reduce the monthly cost, it could be useful in prolonging battery life. The high power rates observed in this work can reduce the lifespan of the battery whereas lower charge rates can prolong battery life. Therefore, future work incorporating battery-health will be explored. We believe that multi-rate charging may offer some flexibility in this scenario. Future work will extend the discrete charge levels in this work to a continuous rate selection.

Because this work presents only a planning framework for a global solution over large stretches of time, it is computationally infeasible to recompute when unplanned events occur. Future work will move this framework toward real-time deployment using a hierarchal approach to control of charging. A precomputed global plan supports the real-time planner by providing top-level guidance. The lower-level real-time planner will adapt to unplanned events by controlling for a return from the current state to the global plan over a finite sliding horizon.

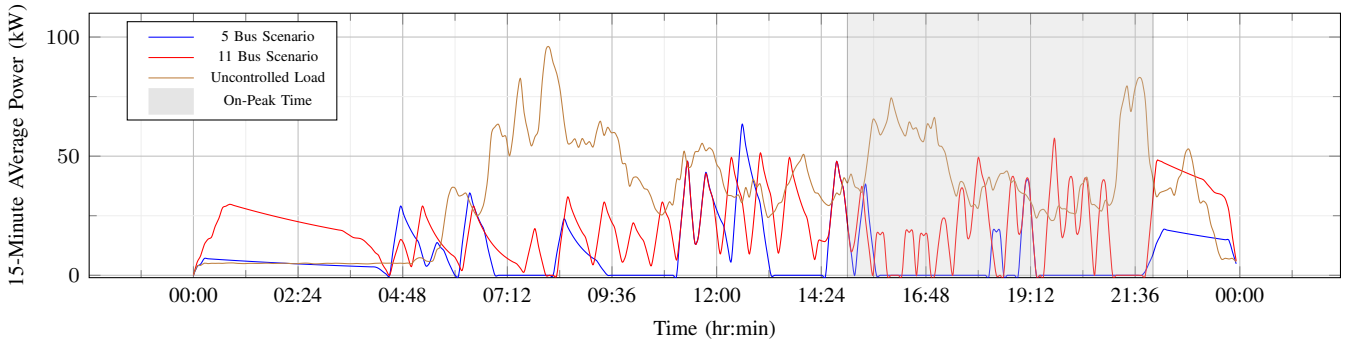

Fig. 21: Comparison of the loads for a 5 and 11 bus scenario with one overhead charger.

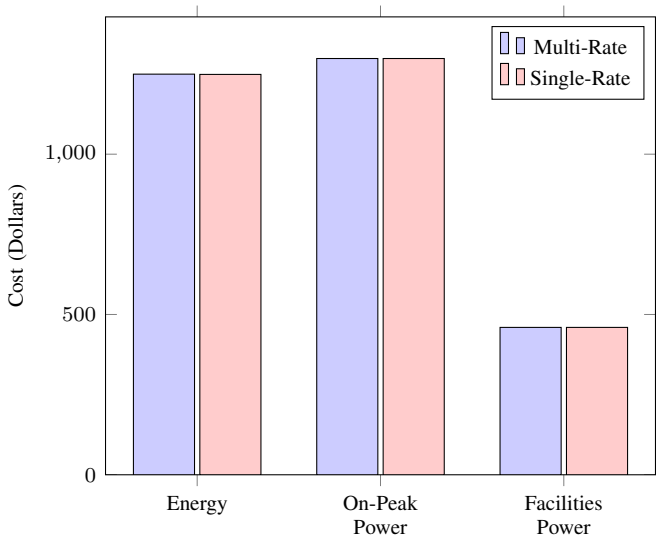

Fig. 22: Cost comparison between a multi-rate and single-rate charge schedule

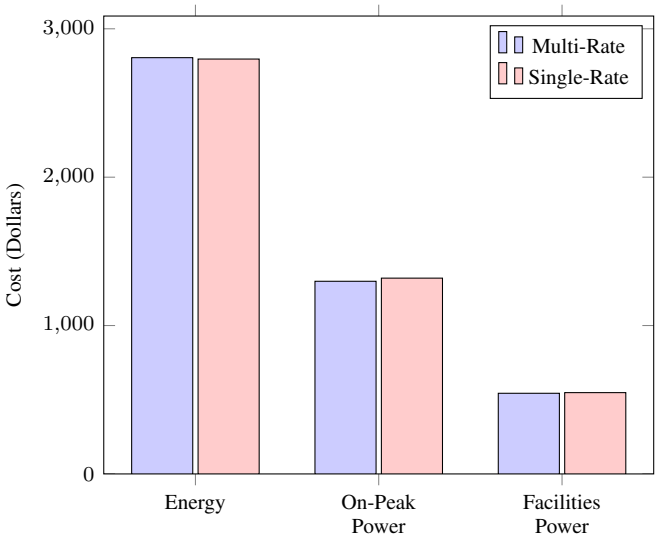

Fig. 23: Cost comaprison between multi and single rate charging for a 35 bus 6 charger scenario.

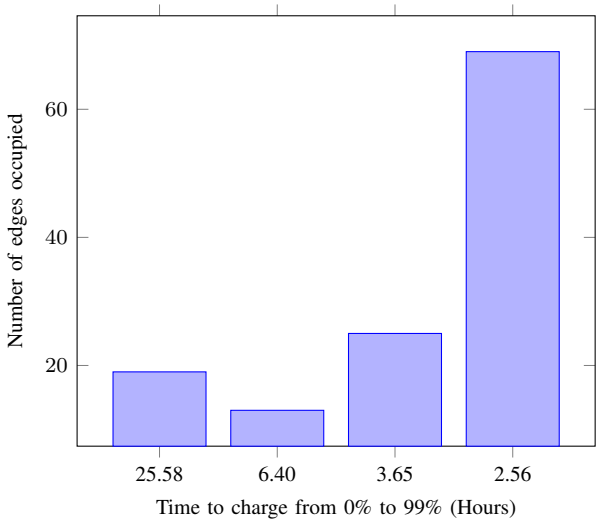

Fig. 24: Histogram of charge rates, where each rate is described by how must time it would take to charge a bus from 0% to 99%.

REFERENCES

[1] Avishan Bagherinezhad et al. "Spatio-Temporal Electric Bus Charging Optimization With Transit Network Constraints". In: *IEEE Transactions on Industry Applications* 56.5 (Sept. 2020), pp. 5741–5749. ISSN: 0093-9994, 1939-9367. DOI: 10.1109/TIA.2020.2979132. URL: https://ieeexplore.ieee.org/document/9028116/ (visited on 11/13/2021).

[2] Bhagyashree J Balde and Arghya Sardar. "Electric Road system With Dynamic Wireless charging of Electric buses". In: *2019 IEEE Transportation Electrification Conference (ITEC-India)*. 2019 IEEE Transportation Electrification Conference (ITEC-India). Bengaluru, India: IEEE, Dec. 2019, pp. 1–4. ISBN: 978-1-72813-169-6. DOI: 10.1109/ITEC-India48457.2019.ITECINDIA2019-251. URL: https://ieeexplore.ieee.org/document/9080859/ (visited on 11/18/2021).

[3] T. Boonraksa et al. "Impact of Electric Bus Charging on the Power Distribution System a Case Study IEEE 33 Bus Test System". In: *2019 IEEE PES GTD Grand International Conference and Exposition Asia*

(GTD Asia). 2019 IEEE PES GTD Grand International Conference and Exposition Asia (GTD Asia). Bangkok, Thailand: IEEE, Mar. 2019, pp. 819–823. ISBN: 978-1-5386-7434-5. DOI: 10.1109/GTDAsia.2019.8716023. URL: https://ieeexplore.ieee.org/document/8716023/ (visited on 11/13/2021).

[4] Qifu Cheng et al. "A smart charging algorithm-based fast charging station with energy storage system-free". In: *CSEE Journal of Power and Energy Systems* (2020). ISSN: 20960042, 20960042. DOI: 10.17775/CSEEJPES.2020.00350. URL: https://ieeexplore.ieee.org/stamp/stamp.jsp?tp=&arnumber=9171658 (visited on 11/19/2021).

[5] Bálint Csonka. "Optimization of Static and Dynamic Charging Infrastructure for Electric Buses". In: *Energies* 14.12 (June 13, 2021), p. 3516. ISSN: 1996-1073. DOI: 10.3390/en14123516. URL: https://www.mdpi.com/1996-1073/14/12/3516 (visited on 11/13/2021).

[6] Sanchari Deb, Karuna Kalita, and Pinakeshwar Mahanta. "Impact of electric vehicle charging stations on reliability of distribution network". In: *2017 International Conference on Technological Advancements in Power and Energy (TAP Energy)*. 2017 International Conference on Technological Advancements in Power and Energy (TAP Energy). Kollam: IEEE, Dec. 2017, pp. 1–6. ISBN: 978-1-5386-4021-0. DOI: 10.1109/TAPENERGY.2017.8397272. URL: https://ieeexplore.ieee.org/document/8397272/ (visited on 11/16/2021).

[7] Nader A. El-Taweel and Hany E. Z. Farag. "Incorporation of Battery Electric Buses in the Operation of Intercity Bus Services". In: *2019 IEEE Transportation Electrification Conference and Expo (ITEC)*. 2019 IEEE Transportation Electrification Conference and Expo (ITEC). Detroit, MI, USA: IEEE, June 2019, pp. 1–6. ISBN: 978-1-5386-9310-0. DOI: 10.1109/ITEC.2019.8790598. URL: https://ieeexplore.ieee.org/document/8790598/ (visited on 11/19/2021).

[8] Qiang Gao et al. "Charging Load Forecasting of Electric Vehicle Based on Monte Carlo and Deep Learning". In: *2019 IEEE Sustainable Power and Energy Conference (iSPEC)*. 2019 IEEE Sustainable Power and Energy Conference (iSPEC). Beijing, China: IEEE, Nov. 2019, pp. 1309–1314. ISBN: 978-1-72814-930-1. DOI: 10.1109/iSPEC48194.2019.8975364. URL: https://ieeexplore.ieee.org/document/8975364/ (visited on 11/19/2021).

[9] Adnane Houbbadi et al. "Optimal Charging Strategy to Minimize Electricity Cost and Prolong Battery Life of Electric Bus Fleet". In: *2019 IEEE Vehicle Power and Propulsion Conference (VPPC)*. 2019 IEEE Vehicle Power and Propulsion Conference (VPPC). Hanoi, Vietnam: IEEE, Oct. 2019, pp. 1–6. ISBN: 978-1-72811-249-7. DOI: 10.1109/VPPC46532.2019.8952493. URL: https://ieeexplore.ieee.org/document/8952493/ (visited on 11/13/2021).

[10] Amra Jahic, Mina Eskander, and Detlef Schulz. "Preemptive vs. non-preemptive charging schedule for large-scale electric bus depots". In: *2019 IEEE PES Innovative Smart Grid Technologies Europe (ISGT-Europe)*. 2019 IEEE PES Innovative Smart Grid Technologies Europe (ISGT-Europe). Bucharest, Romania: IEEE, Sept. 2019, pp. 1–5. ISBN: 978-1-5386-8218-0. DOI: 10.1109/ISGTEurope.2019.8905633. URL: https://ieeexplore.ieee.org/document/8905633/ (visited on 11/16/2021).

[11] Shubham Jain et al. "Battery Swapping Technology". In: *2020 5th IEEE International Conference on Recent Advances and Innovations in Engineering (ICRAIE)*. 2020 5th IEEE International Conference on Recent Advances and Innovations in Engineering (ICRAIE). Jaipur, India: IEEE, Dec. 1, 2020, pp. 1–4. ISBN: 978-1-72818-867-6. DOI: 10.1109/ICRAIE51050.2020.9358366. URL: https://ieeexplore.ieee.org/document/9358366/ (visited on 11/18/2021).

[12] Seog Y. Jeong et al. "Automatic Current Control by Self-Inductance Variation for Dynamic Wireless EV Charging". In: *2018 IEEE PELS Workshop on Emerging Technologies: Wireless Power Transfer (Wow)*. 2018 IEEE PELS Workshop on Emerging Technologies: Wireless Power Transfer (WoW). Montréal, QC, Canada: IEEE, June 2018, pp. 1–5. ISBN: 978-1-5386-2465-4. DOI: 10.1109/WoW.2018.8450926. URL: https://ieeexplore.ieee.org/document/8450926/ (visited on 11/18/2021).

[13] Inaki Ojer et al. "Development of energy management strategies for the sizing of a fast charging station for electric buses". In: *2020 IEEE International Conference on Environment and Electrical Engineering and 2020 IEEE Industrial and Commercial Power Systems Europe (EEEIC / I&CPS Europe)*. 2020 IEEE International Conference on Environment and Electrical Engineering and 2020 IEEE Industrial and Commercial Power Systems Europe (EEEIC / I&CPS Europe). Madrid, Spain: IEEE, June 2020, pp. 1–6. ISBN: 978-1-72817-455-6. DOI: 10.1109/EEEIC/ICPSEurope49358.2020.9160716. URL: https://ieeexplore.ieee.org/document/9160716/ (visited on 11/16/2021).

[14] Kavuri Poornesh, Kuzhivila Pannickottu Nivya, and K. Sireesha. "A Comparative study on Electric Vehicle and Internal Combustion Engine Vehicles". In: *2020 International Conference on Smart Electronics and Communication (ICOSEC)*. 2020 International Conference on Smart Electronics and Communication (ICOSEC). Trichy, India: IEEE, Sept. 2020, pp. 1179–1183. ISBN: 978-1-72815-461-9. DOI: 10.1109/ICOSEC49089.2020.9215386. URL: https://ieeexplore.ieee.org/document/9215386/ (visited on 11/13/2021).

[15] Nan Qin et al. "Numerical analysis of electric bus fast charging strategies for demand charge reduction". In: *Transportation Research Part A: Policy and Practice* 94 (Dec. 2016), pp. 386–396. ISSN: 09658564. DOI: 10.1016/j.tra.2016.09.014. URL: https://linkinghub.elsevier.com/retrieve/pii/S096585641630444X (visited on 11/13/2021).

[16] *Rocky Mountain Power Electric Service Schedule No. 8 State of Utah*. URL: https://www.

rockymountainpower . net / content / dam / pcorp / documents / en / rockymountainpower / rates - regulation / utah / rates / 008_Large_General_Service_1_000_ kW_and_Over_Distribution_Voltage . pdf (visited on 02/03/2022).

[17] Daniel Stahleder et al. "Impact Assessment of High Power Electric Bus Charging on Urban Distribution Grids". In: *IECON 2019 - 45th Annual Conference of the IEEE Industrial Electronics Society*. IECON 2019 - 45th Annual Conference of the IEEE Industrial Electronics Society. Lisbon, Portugal: IEEE, Oct. 2019, pp. 4304–4309. ISBN: 978-1-72814-878-6. DOI: 10 . 1109/IECON.2019.8927526. URL: https://ieeexplore. ieee.org/document/8927526/ (visited on 11/16/2021).

[18] Ran Wei et al. "Optimizing the spatio-temporal deployment of battery electric bus system". In: *Journal of Transport Geography* 68 (Apr. 2018), pp. 160–168. ISSN: 09666923. DOI: 10.1016/j.jtrangeo.2018.03. 013. URL: https://linkinghub.elsevier.com/retrieve/pii/ S0966692317306294 (visited on 11/13/2021).

[19] Justin Whitaker et al. "A Network Flow Approach to Battery Electric Bus Scheduling". In: (2021), p. 10.

[20] Xian Zhang and Guibin Wang. "Optimal dispatch of electric vehicle batteries between battery swapping stations and charging stations". In: *2016 IEEE Power and Energy Society General Meeting (PESGM)*. 2016 IEEE Power and Energy Society General Meeting (PESGM). Boston, MA, USA: IEEE, July 2016, pp. 1–5. ISBN: 978-1-5090-4168-8. DOI: 10 . 1109 / PESGM . 2016 . 7741893. URL: http://ieeexplore.ieee.org/document/ 7741893/ (visited on 11/18/2021).

[21] Dan Zhou et al. "Optimization Method of Fast Charging Buses Charging Strategy for Complex Operating Environment". In: *2018 2nd IEEE Conference on Energy Internet and Energy System Integration (EI2)*. 2018 2nd IEEE Conference on Energy Internet and Energy System Integration (EI2). Beijing: IEEE, Oct. 2018, pp. 1–6. ISBN: 978-1-5386-8549-5. DOI: 10.1109/EI2. 2018 . 8582378. URL: https : / / ieeexplore . ieee . org / document/8582378/ (visited on 11/13/2021).